International Journal of Rotating Machinery, 10: 33–44, 2004

ISSN: 1023-621X print
DOI: 10.1080/10236210490258052

Aerodynamic and Performance Behavior of a Three-Stage High Efficiency Turbine at Design and Off-Design Operating Points

M. T. Schobeiri, J. L. Gilarranz, and E. S. Johansen
Turbomachinery Performance and Flow Research Laboratory, Texas A&M University, College Station, Texas, USA

This article deals with the aerodynamic and performance behavior of a three-stage high pressure research turbine with 3-D curved blades at its design and off-design operating points. The research turbine configuration incorporates six rows beginning with a stator row. Interstage aerodynamic measurements were performed at three stations, namely downstream of the first rotor row, the second stator row, and the second rotor row. Interstage radial and circumferential traversing presented a detailed flow picture of the middle stage. Performance measurements were carried out within a rotational speed range of 75% to 116% of the design speed. The experimental investigations have been carried out on the recently established multi-stage turbine research facility at the Turbomachinery Performance and Flow Research Laboratory, *TPFL*, of Texas A&M University.

Keywords

Development in the field of turbomachinery computational fluid dynamics (CFD) has reached an advanced level that allows a detailed computation of the complex three-dimensional viscous flow field through a turbomachinery stage using Navier-Stokes codes. Numerous published cases demonstrate the capability of different CFD-methods to calculate various flow quantities in a remarkably detailed fashion. The efficiency and loss calculations, however, reveal noticeable disagreement between the experimental and computational results. The detailed 3-D flow pictures delivered by viscous flow solvers display the source and location of the total pressure losses and entropy distribution within the blade channel, particularly at the blade hub and tip regions. Based on these results, the turbine aerodynamicist is able to reconfigure the blade geometry to reduce the profile and the secondary flow losses. The latter is especially relevant for high pressure (HP) turbine design with relatively small aspect ratios where the secondary flow losses significantly contribute to the reduction of the stage efficiency. In recent years, the power generation turbine manufacturers have been increasingly focusing their efforts on reducing the secondary flow losses of HP-turbine blades by implementing the information obtained from the Navier-Stokes flow simulations. To account for the discrepancy mentioned above, the Navier-Stokes codes are frequently *calibrated*. The calibration process may provide a temporary matching solution for cases in which experimental results are available. However, it is not appropriate for a priori predicting of the efficiency of new designs. The disagreement between the Navier-Stokes based efficiency calculations and the measurements, however, does not allow the engine manufacturer to issue efficiency and performance guaranty without thoroughly testing their new design. Considering the physical aspects of the computation, among other things, two major issues may be considered primarily responsible for the above discrepancy, namely the turbulence modeling and the modeling of the laminar-turbulent boundary layer transition process. The latter directly impacts the accuracy of the loss, efficiency and heat transfer calculations of the blade and thus the turbomachinery stage.

BACKGROUND: UNSTEADY BOUNDARY LAYER TRANSITION

To quantify the effect of unsteady boundary layer transition on turbine efficiency the first author initiated a comprehensive unsteady boundary layer research program at Texas A&M University, where he and his co-workers studied the development

Received 25 June 2002; accepted 1 July 2002.
The research reported in this paper was supported by the Siemens-Westinghouse Power Corporation. The authors would like to thank Dr. S. Chen, Mr. H. Martin, Mr. A. Pallotta, and the Siemens-Westinghouse Power Corporation.
Address correspondence to M. T. Schobeiri, Texas A&M University, Dept. of Mechanical Engineering, College Station, TX 77843-3123. E-mail: tschobeiri@mengr.tamu.edu

of steady and unsteady wake development under turbomachinery specific conditions.

Schobeiri et al. (1994) investigated the phenomenon of steady wake development and decay and established a comprehensive theoretical frame-work. Schobeiri and his co-workers also extended the theoretical work by Schobeiri et al. (1995a) to a relative frame of reference to explain the development and decay of unsteady wakes. Schobeiri et al. (1995b) experimentally investigated the effects of periodic unsteady wake passing frequency on the boundary layer transition and its development along the concave surface of a constant curvature plate at zero pressure gradient. In a continuing effort, Schobeiri et al. (1998) presented a detailed experimental study of the behavior of the unsteady boundary layer of a turbine cascade with a chord length of $c = 281.8$ mm. Wright and Schobeiri (1999) complemented the above unsteady boundary layer studies by performing heat transfer investigations using liquid crystal measurement techniques. Based on the aerodynamic and heat transfer experimental results, Chakka and Schobeiri (1999) developed a fully unsteady boundary layer transition model. To validate the above unsteady transition, Schobeiri et al. (1998) applied the model to an unsteady turbine cascade and found excellent agreement between theory and the experiment.

TURBINE STAGE INVESTIGATIONS

In a recent study, Emund et al. (1999) computationally investigated the adjacent blade-row effects in a 1.5 stage axial flow turbine. The authors used two different codes and compared the computational results with the experimental ones obtained downstream of each blade row. Both codes use the algebraic (Baldwin-Lomax) model with a prescribed transition location at 60 percent. Their computations show that the flow distribution is qualitatively well predicted. The level of the total pressure distribution, however, is not predicted accurately. Although the total pressure loss coefficients are not shown in the study, the computed and the measured total pressures indicate that the resulting total pressure loss coefficients for the rows under investigation suggest noticeable differences between computation and experiment. The accurate prediction of stator and rotor row loss coefficients, however, is a prerequisite for an accurate efficiency calculation. In an experimental study on a multistage low-pressure (LP) turbine, Arndt (1993) illustrated the profound influence of the wake-induced rotor-stator and rotor-rotor interaction on the flow through downstream blade rows. Arndt showed that the interaction results in strong amplitude-modulated periodic and turbulent velocity fluctuations downstream of every rotor blade row. Using surface mounted hot film anemometers, Hodson et al. (1993) performed experimental investigations on a multistage LP-turbine. Based on their results, they suggested that the presence of the wakes influenced the transition in a separated flow region. As a consequence, they argued, that a design produced by the application of steady flow methods might not represent the optimum that can be achieved.

In a four-part study, Halstead et al. (1995) investigated the boundary layer development in axial compressors and turbines. Part 3 of the study focused on unsteady flow and the effects of the wakes on the performance of LP-turbines. The study presented and interpreted the data from the surface hot film probes and the boundary layer survey for baseline operating conditions. The study by Halstead et al. (1995) has contributed to better understanding the flow physics through an LP-turbine component.

To address the major turbine performance and flow research issues, the principal author of this paper developed and designed a state-of-the-art multipurpose turbine research facility with a versatile research turbine as its core component. The modular structured design of the research turbine enables the incorporation of up to four turbine stages. The stator and rotor blades may be of any arbitrary design, ranging from zero degree reaction cylindrical blades to higher reaction 3-D blades. They also may be test blades of high, intermediate, or low pressure turbine units. The facility is capable of accurately measuring the efficiency and performance of the entire turbine engine. In particular, the sophisticated interstage traversing system provides a detailed flow picture of the turbine middle stage. The paper presents the results of the experiments performed on a three-stage HP-turbine with 3-D blades.

HP-TURBINE EXPERIMENTAL RESEARCH

Research Facility

The overall layout of the test facility is shown in Figure 1, it consists of (1) a 300-kW electric motor connected to a frequency controller which drives the compressor component, (2) a three-stage centrifugal compressor supplies air with a maximum pressure difference of 55 kPa and a volume flow rate of 4 m^3/s. The compressor operates in suction mode and its pressure and volume flow can be varied by a frequency controller from 0 to 66 Hz. The compressor and its drive are located inside a housing which is outside the test cell. A pipe with a transition piece connects the compressor to a Venturi mass flow meter, (3) used to measure the mass flow through the turbine component. The exit diffuser-flow straightener system (4) serves as a smooth transition piece between the turbine component and the Venturi. (5) A three-stage turbine with a fully automated data acquisition system. (6) The turbine inlet has an integrated heater that prevents condensation of water from humid air expanding through the turbine during the test. (7) The turbine shaft is connected through a flexible coupling with one end of a high precision torque meter that has a maximum rotational speed of 8500 rpm and a maximum torque of 677.9 Nm. The accuracy of this torque meter is $\pm 0.02\%$ of full scale. The other end of the torque meter is coupled via a second flexible coupling with an eddy current low inertia dynamometer, (8) with the maximum power of 150 kW, a maximum torque of 500 Nm, a maximum rotational speed of 8000 rpm, a torque accuracy of ± 1.25 Nm (a minimum requirement: 0.25% of a full scale load), and a rotational speed accuracy of ± 1 rpm. The dynamometer is

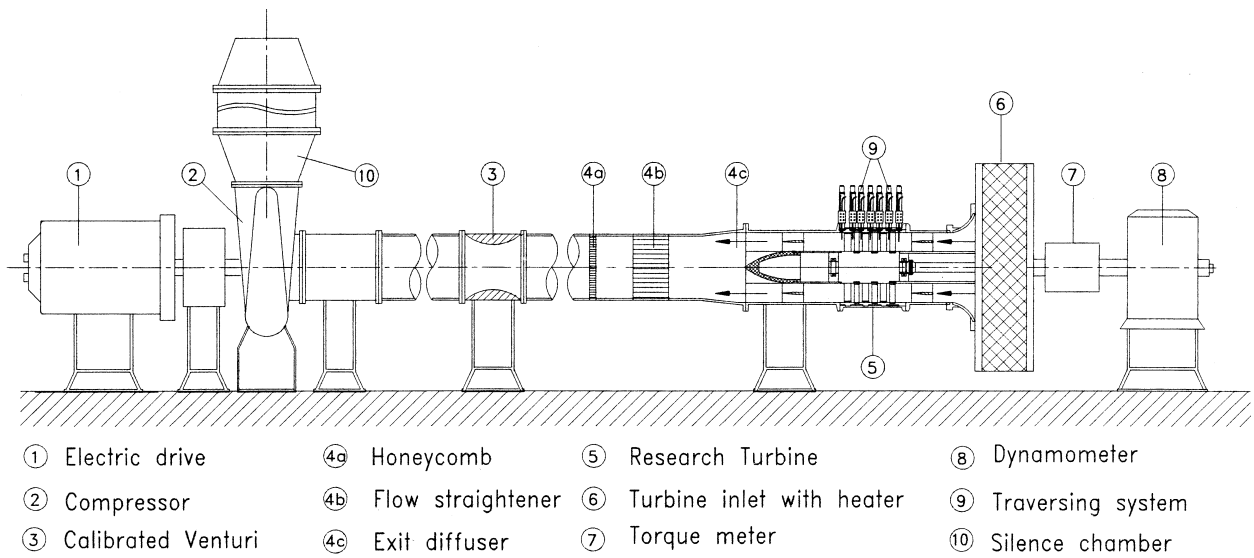

FIGURE 1
The *TPFL* research turbine facility with its components, the circumferential traversing system (9) is driven by another traversing system sitting on a frame and is perpendicular to this plane.

controlled by a Texcel V4-EC controller including an RS-232 port for connecting to a data acquisition computer. The major components of this facility were chosen so that the engine efficiency accuracy requirements of less than 0.5% are satisfied.

The Three-Stage Research Turbine, Instrumentation

The turbine component shown in Figure 2 is a three-stage air turbine with the dimensions specified in Table 1. To achieve a high degree of versatility, the turbine was designed with a casing that incorporates stator rings. It also incorporates three T-rings for sealing the three 90-degree circumferential traversing slots, as seen in Figure 3. The rotor blades are shrouded and attached to the rotor cylinder, which is connected to the shaft via two locking mechanisms, Figure 4 top. This design allows the entire rotor unit to be disassembled and to reuse the shaft and the bearings, when replacing the cylinder for another turbine type. The versatile turbine design allows clocking the stator rings individually and externally without disassembling the turbine. Table 1 provides the operating range of the turbine. For the performance instrumentation, combined total pressure and total temperature rakes are used upstream of the first stator row and downstream of the last rotor row. At the inlet, the rakes were located radially at 45°, 135°, 225°, and 315°. Each rake consists of 4 total pressure and 3 total temperature probes that are equidistantly distributed in the radial direction. The total pressure probes are of the Pitot tube types, and the total temperature probes are calibrated J-type thermocouples. The calibration curves for the thermocouples are implemented into the performance data reduction program. To reduce the wake thickness originating from the trailing edge of the inlet rakes, the rakes are shaped aerodynamically with a round leading edge and a sharp trailing edge. The exit rakes are located radially with the same spacing as the inlet rakes, but offset from them in order to prevent interference with the inlet rake wakes. Wall static pressure taps are arranged at the top and bottom half of the main casing and on the T-rings, as well as on the stator rings. In addition, total temperature and pressure probes are mounted on the leading edge stagnation points of two diametrically opposed stator blades of the second and third stator rows. For the mass flow measurement, a calibrated Venturi flow meter was used. The turbine engine has the capability of radially traversing the flow field at stations 1 through 7 (Figure 3) and

TABLE 1
Turbine Research Facility Data

Items	Specifications
Stage number	N = 3
Tip diameter	$D_t = 685.8$ mm
Hub diameter	$D_h = 558.8$ mm
Blade height	Bh = 63.5 mm
Blade number	Stator 1 = 58
Blade number	Rotor 1 = 46
Power	$P = 80.0$–110.0 kW
Mass flow	$\dot{m} = 3.728$ kg/s
Speed range	$n = 1800$–2800 rpm
Inlet pressure	$p_{in} = 101.356$ kPa
Exit pressure	$p_{ex} = 71.708$ kPa
Stator 2 = 52	Stator 3 = 56
Rotor 2 = 40	Rotor 3 = 44

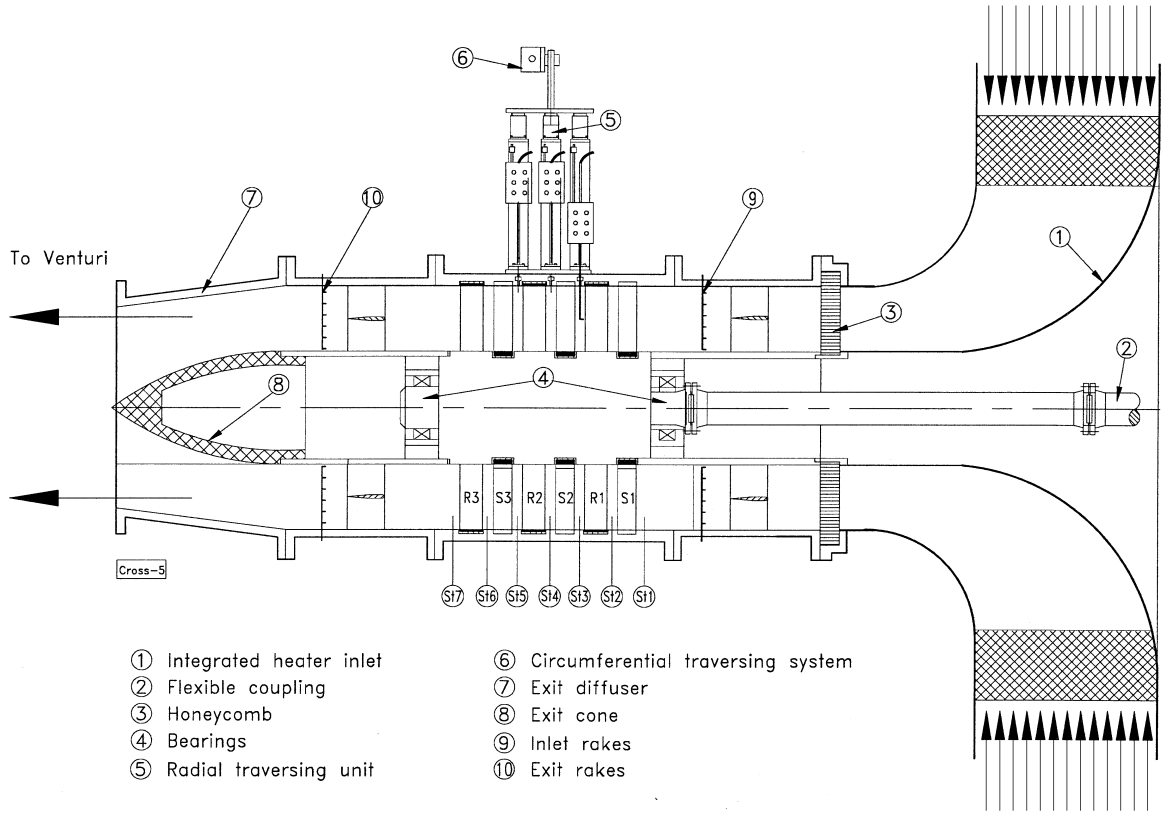

FIGURE 2
A schematic cross section of the *TPFL*-research turbine with its major components.

circumferentially/radially traversing at stations 3, 4, and 5. The data are used to generate the total and static pressure contours, velocity components, flow angles, the spanwise distribution of total pressure loss coefficients, and the efficiency for each row. For this purpose, three L-shaped five-hole probes were used. The first and the third probes were installed at stations 3 and 5 and calibrated at low subsonic Mach number (M = 0.1), where as the second one installed at station 4 was calibrated taking into account the compressibility effect due to the higher subsonic Mach number (M = 0.3). A non-nulling calibration method was applied and the five-hole probes were independently calibrated in a fully automated calibration facility. Each of the probes was placed in an angular indexing mechanism and then pitched and yawed through the range of angles (-20° to 20° in pitch and -30° to 30° in yaw) in 2 degree increments. The calibration facility probe indexing mechanism uses two stepper motors that are computer controlled to achieve a very fine angle resolution. A computer algorithm that creates a user-specified grid of pitch and yaw angles is used to control these stepper motors. The same algorithm also records the pressures from the PSI-9016 pressure scanner and puts the pressures from the five-hole probe, with the corresponding pitch and yaw angles, and the calibration nozzle total pressure into a data file. This data file is then used to create the calibration surfaces for the specific probes that are later used to determine the velocity components and vectors at stations 3, 4, and 5 of the turbine engine. The three probes are turned at specified angles δ_3, δ_4, and δ_5 (Figure 4 bottom). The absolute and relative flow angles and velocity components of the turbine rows are calculated by implementing the probe adjustment angle δ_i for each of the three probes at stations 3, 4 and 5, respectively.

EXPERIMENTAL RESULTS

Interstage Traversing

Interstage traversing was performed at rotational speeds of 1800 to 2800 rpm. Figure 4 bottom shows the locations of the traversing at stations 3, 4, and 5. As shown in Figures 1 and 3, three five-hole probes are mounted on three traversing systems with a decoder and encoder for accurate probe positioning. Each system is individually connected to a controller with feedback that can move the probe with a precision of 1/400 mm (2.5 μm). The three traversing systems are mounted on the top of a base plate, which is connected with the three T-rings that are installed within the casing. The base plate with the three traversing systems constitutes a traversing unit, which is connected with a fourth traversing system placed on top of a frame and moves the unit in the circumferential direction

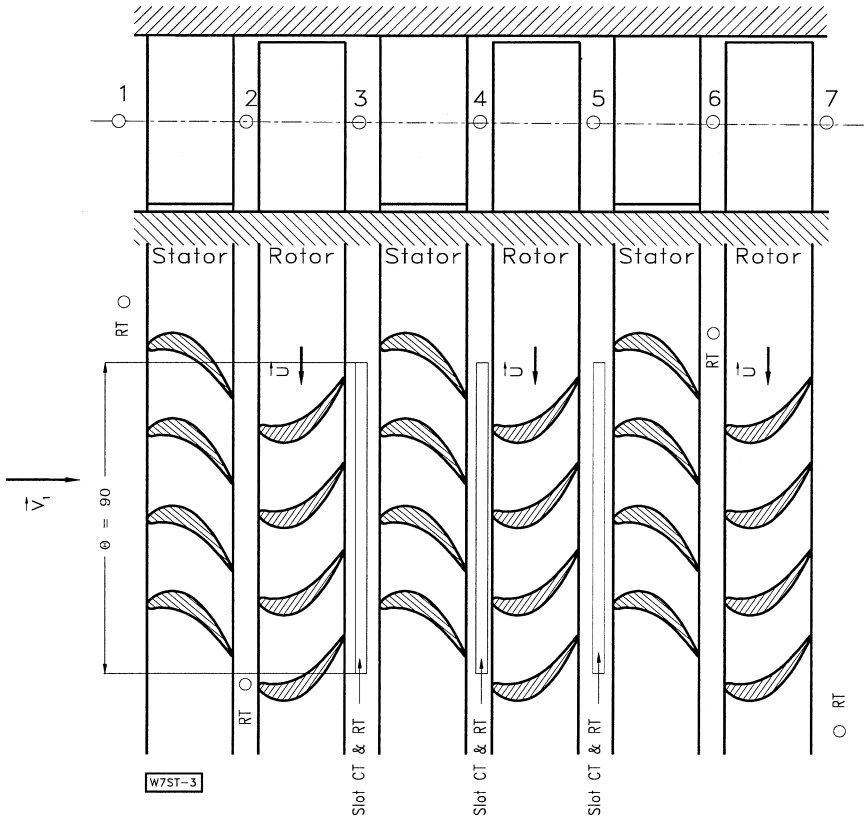

FIGURE 3
Location of the T-ring slots for circumferential and radial traversing, CT = Circumferential Traversing, RT = Radial Traversing.

(Figure 2). Interstage traversing was performed from 1 mm underneath the hub diameter to 1 mm above the tip diameter. This was possible because of the grooves at the rotor hub and the T-rings.

Comprehensive performance measurements and interstage traversing were carried out at the above rotational speeds. For the design point case, the absolute flow angle distributions downstream of the second stator at station 4 (Figure 5) and the relative flow angles downstream of the first and second rotor row at stations 3 and 5 (Figure 6) exhibit a relatively moderate variation from hub to tip. These angles are plotted in Figures 5 and 6 as a function of the immersion ratio $R = (r - r_h)/(r_t - r_h)$. Downstream of the first and second rotor row at station 3 and 5, the absolute flow angles undergo major changes from hub to tip. Except for the immersion ratio range between $R = 0.3$ to 0.6, the absolute flow angles α_3 and α_5 experience changes in the range of over 5°. The same is true for the relative flow angle β_4. In contrast, the stator absolute flow angle α_4 undergoes a moderate change that corresponds to the stator exit metal angle. The radial angle γ downstream of the second stator row and the second rotor row, stations 4 and 5, are close to zero over half of the blade span.

Absolute and relative flow Mach numbers as function of immersion ratios are shown in Figures 7 and 8. Uniform low subsonic absolute Mach numbers around 0.1 are encountered downstream of the first and second rotor, stations 3 and 5, whereas the second stator exit Mach number, at station 4, is generally above 0.25. Changing the frame of reference from the absolute frame into the relative one, higher uniform Mach numbers at stations 3 and 5 are shown in Figure 8 that indicate a higher relative flow deflection at the rotor exit.

Considering the flow angles, Figure 9 exhibits the distribution of the axial velocity component, which is responsible for mass flow distribution in the spanwise direction. Disregarding the points close to the hub affected by the low energy boundary layer, downstream of the stator at station 4, a high axial velocity component is encountered in the hub region. This counteracts the production of high strength secondary vortices, which are present in conventional cylindrical blades near the hub and the tip. This velocity component decreases with increasing the immersion ratio until it reaches the ratio of $R = 0.65$. Here again, a substantial increase starting at $R = 0.7$ helps to reduce the tip secondary vortex strength contributing to the overall reduction of secondary flow losses.

The interstage traversing provides the entire flow quantities, from which the absolute and relative total pressures and thus the total pressure loss coefficients for the stator and the rotor can be determined. For this purpose, first the traversed

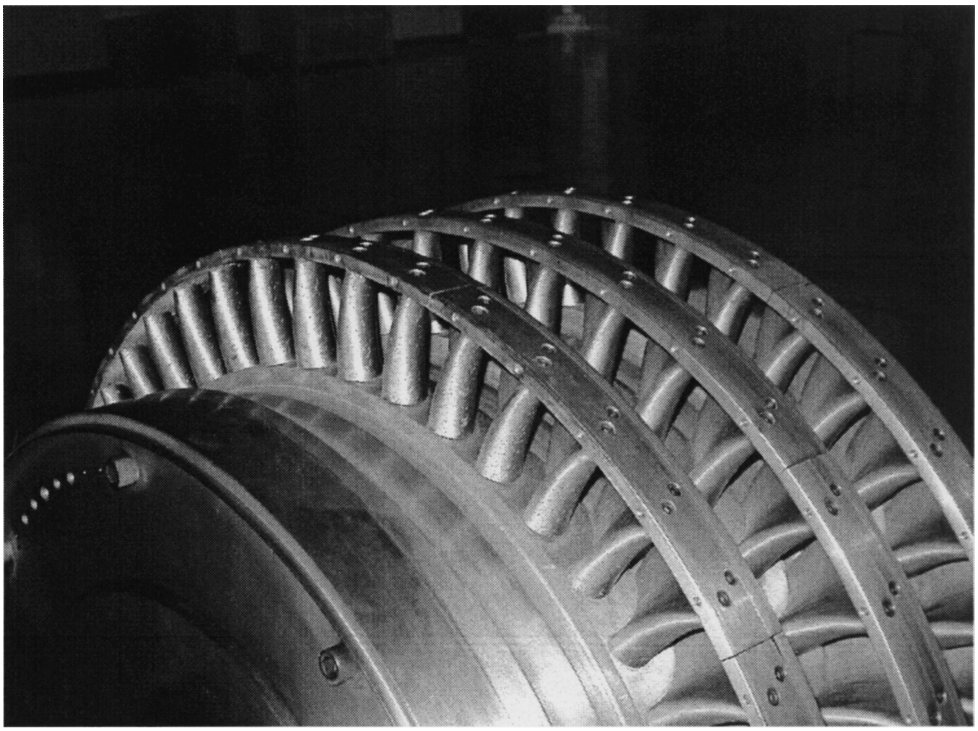

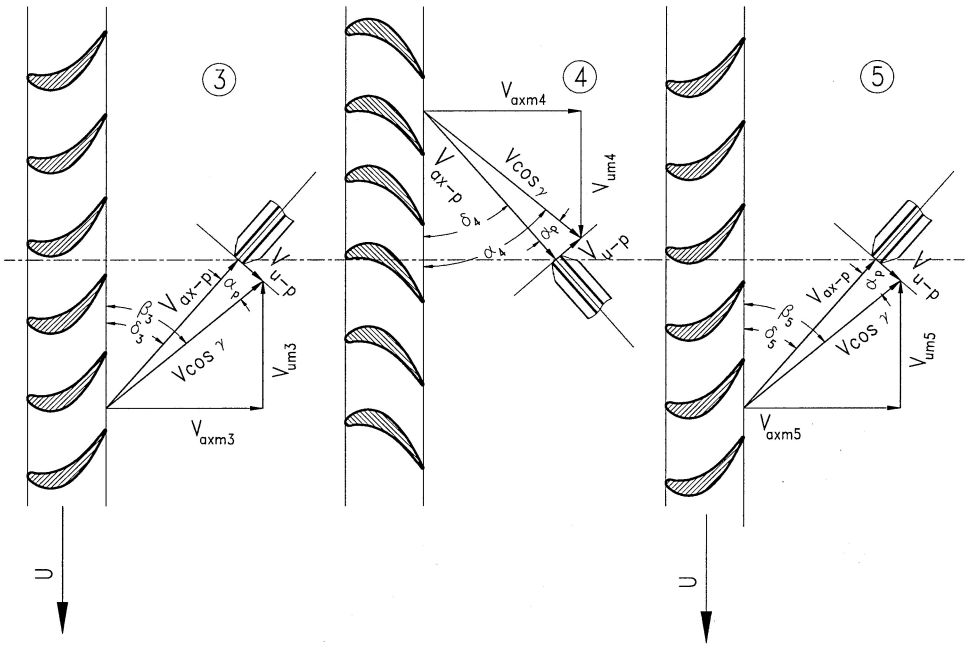

FIGURE 4

Rotor unit of the *TPFL*-turbine research facility, bottom: angular position of the five-hole probes at station 3, 4, and 5.

quantities are averaged in the circumferential direction. The averaged quantities must be consistent with conservation laws of thermodynamics and fluid mechanics. The significance of an appropriate averaging technique and its impact on the results has been well known in the turbomachinery community for more than three decades and does not need to be reviewed here (see extensive review by Traupel, 1977). A simple *consistent averaging technique* that yields consistent results at a plane

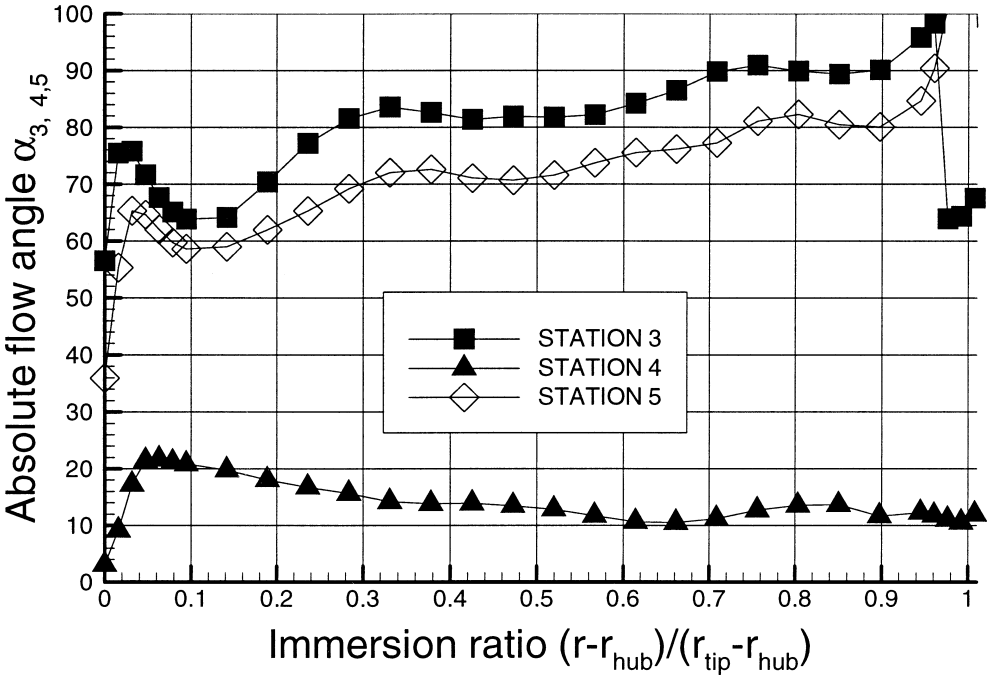

FIGURE 5
Radial distribution of the absolute flow angle at stations 3, 4, and 5.

under inhomogeneous flow conditions was introduced by Dzung (1971). This averaging method is considered as standard averaging technique (see recent papers by Emund et al., 1999; Day et al., 1999). For a given control volume, the averaging technique by Dzung yields integral quantities that are inherently consistent with the conservation laws. To obtain consistently averaged data for distributed quantities in the radial direction, the technique required a further enhancement, which was done at *TPFL*.

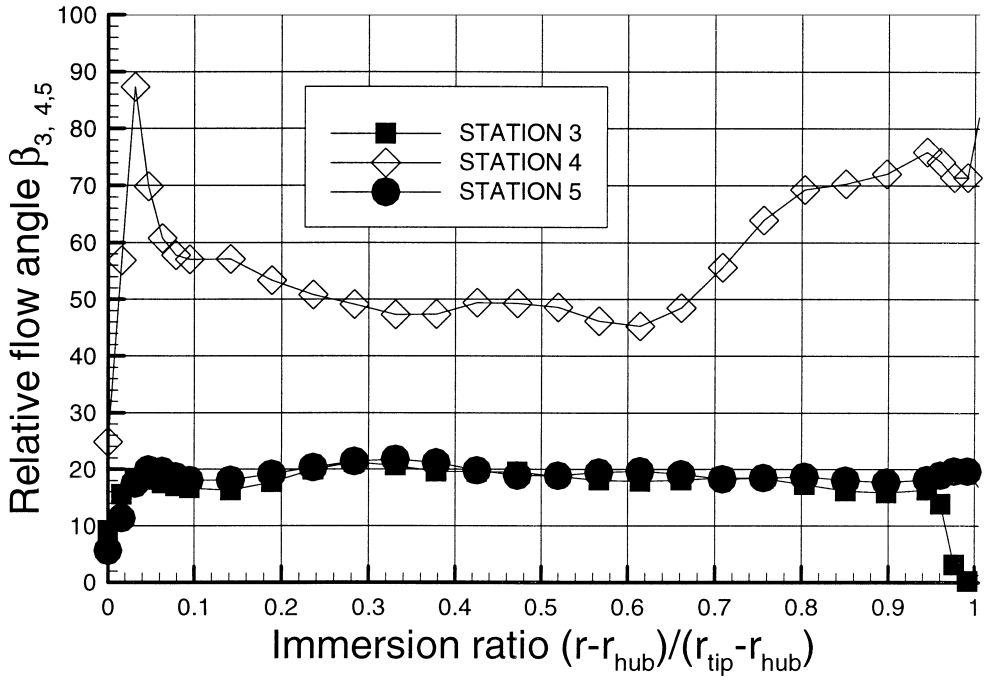

FIGURE 6
Radial distribution of the relative flow angle at stations 3, 4, and 5.

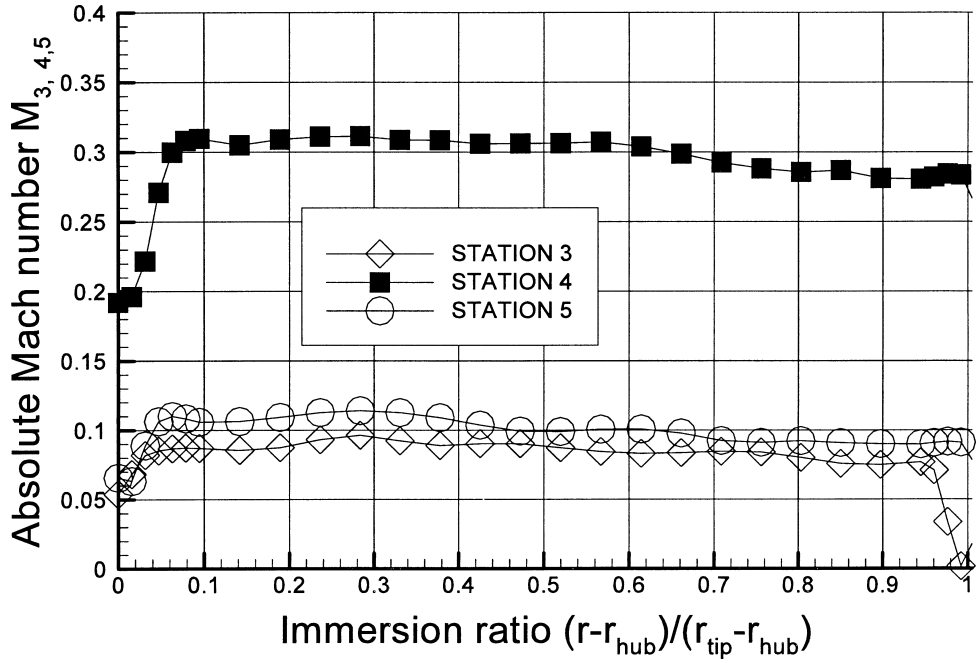

FIGURE 7
Radial distribution of the absolute Mach number at stations 3, 4, and 5.

Using circumferentially consistently averaged quantities, we define the total pressure loss coefficients for stator and rotor as:

$$\zeta_{Stator} = \frac{P_3 - P_4}{P_3 - P4}, \zeta_{Rotor} = \frac{P_{4r} - P_{5r}}{P_{4r} - P_5} \quad [1]$$

with P_3, P_4 as the absolute total pressure upstream and downstream of the stator, $P_{4r} - P_{5r}$ as the relative total pressure upstream and downstream of the rotor, and p_4, p_5 as the static pressure at stations 4 and 5. Figure 10 shows the stator and rotor loss coefficients normalized with the corresponding loss coefficient in midheight, $\zeta_{0.5}$. As seen, a uniform total pressure

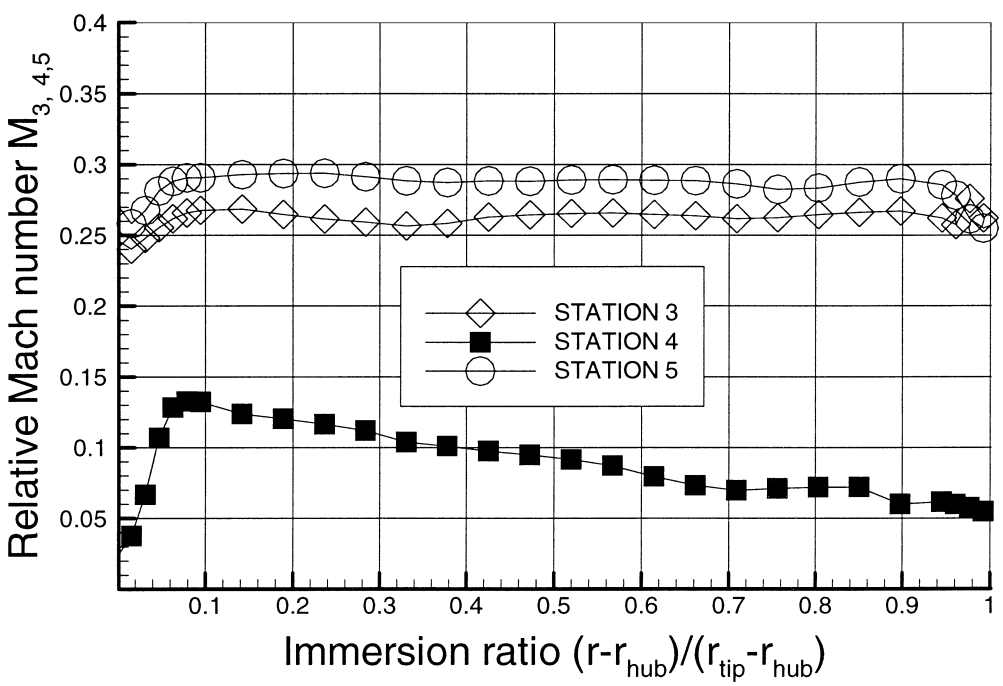

FIGURE 8
Radial distribution of the relative Mach numbers at stations 3, 4, and 5.

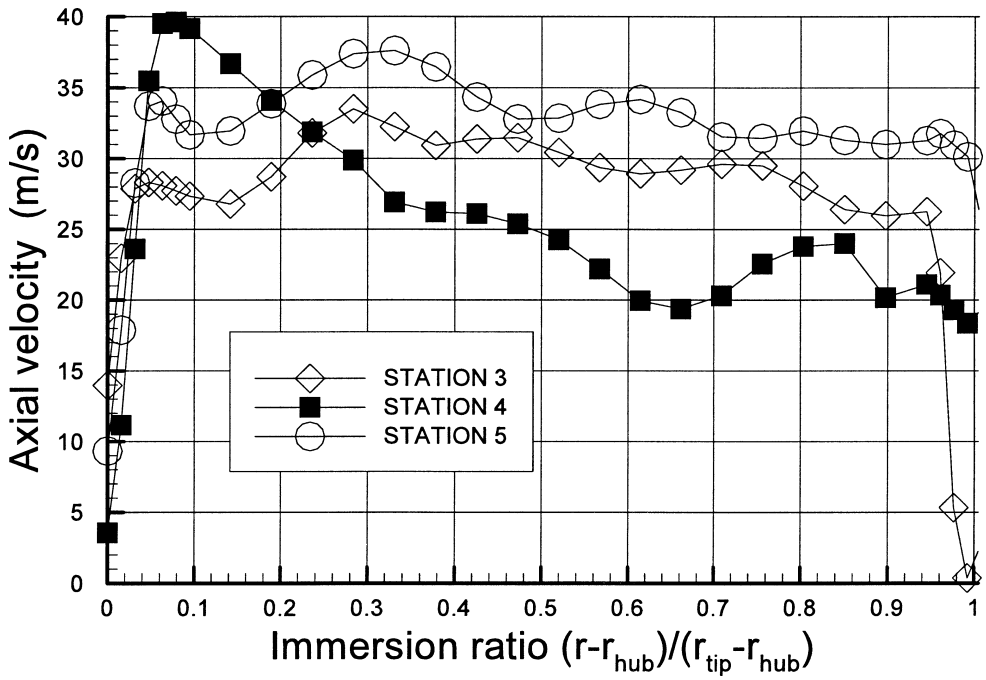

FIGURE 9
Radial distribution of the axial velocity component at stations 3, 4, and 5.

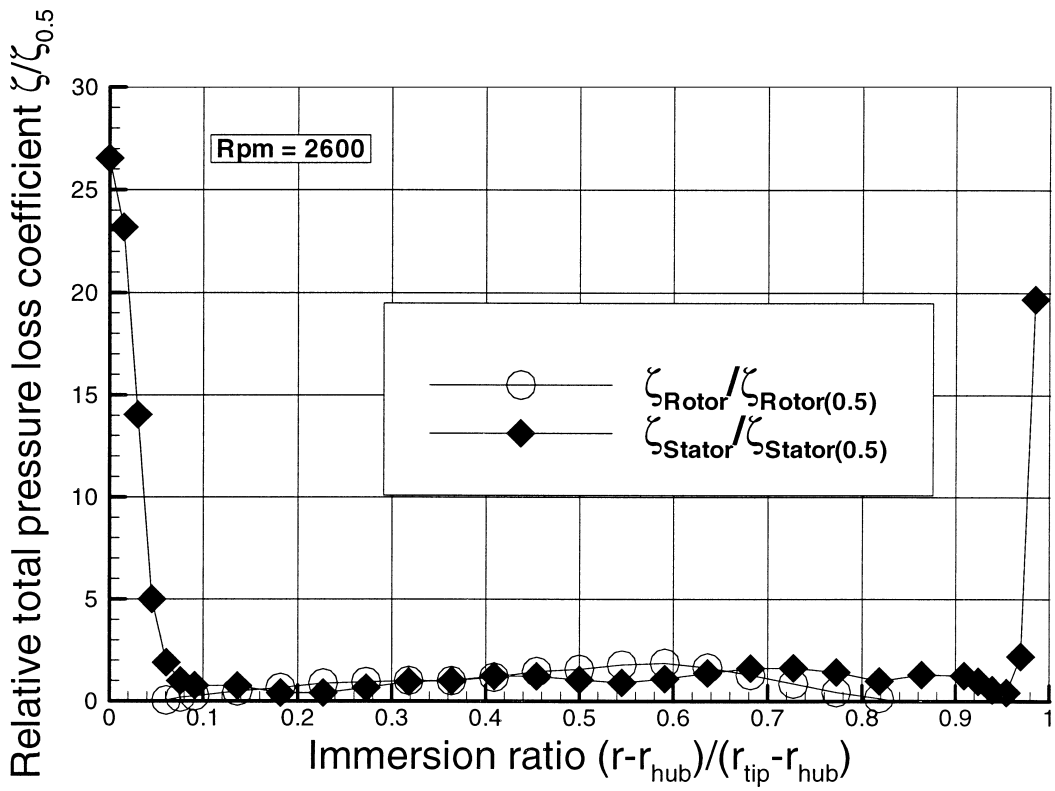

FIGURE 10
Radial distribution of the relative total pressure loss coefficients for stator and rotor row.

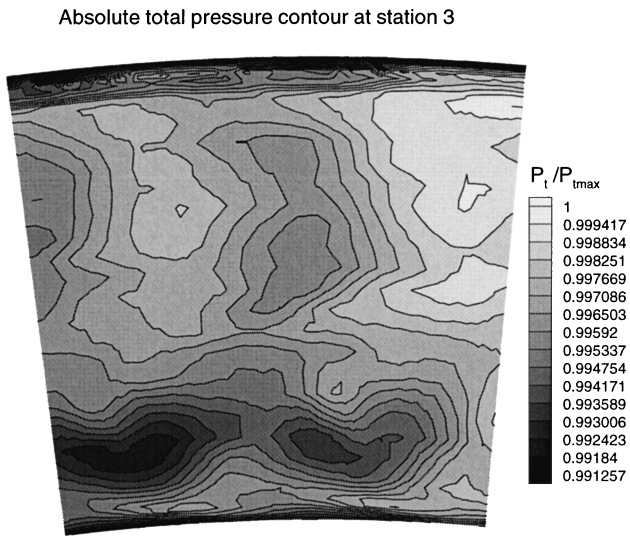

(a)

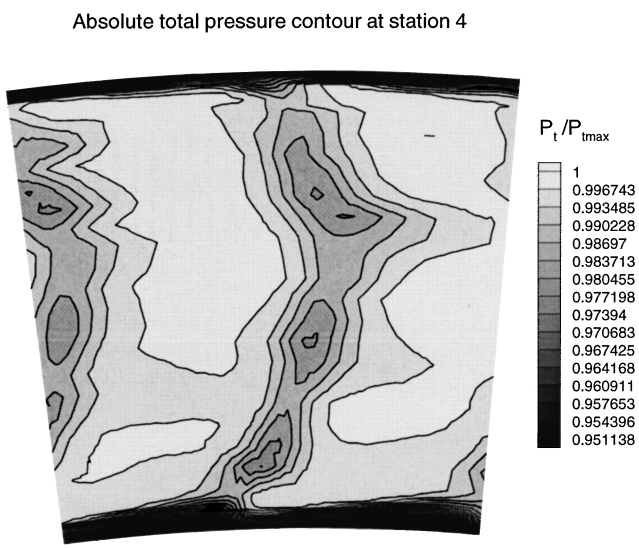

(b)

FIGURE 11a,b
Dimensionless total pressure contour at station 5 with P_{tmax} as the maximum total pressure within the domain.

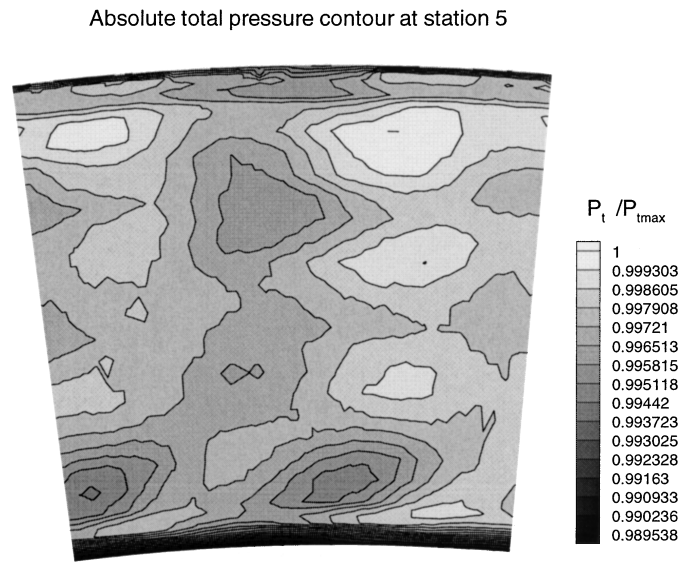

(c)

FIGURE 11c
Dimensionless total pressure contour at station 5 with P_{max} as the maximum total pressure.

loss coefficient is extended over 90% of the blade span. The secondary flow losses are confined to two narrow regions close to the hub and the tip. Qualitative comparison with the earlier investigations by Berg (1973) and the very recent study by Emund et al. (1999) shows that the implementation of a 3-D configuration design has reduced the secondary flow losses considerably. Berg (1973) in his study, which is probably one of the most comprehensive studies concerning the secondary flow losses in HP-turbine blades, used a series of cylindrical blades for his secondary flow loss investigations. His loss coefficient plots show two very pronounced peaks located at 18% and 85% of the blade span for all five rotors he investigated. The low total pressure regions occupied by the secondary flow losses extend from 0% to 30% at the hub and from 80% to 100% at the tip. Similar distributions are found in many LPT-studies such as the one by Schütz (1971). Emund et al. (1999) used Traupel and VKI profiles, which are untwisted blades, for their 1.5-stage investigations. Although Emund et al. (1999) have not presented the total pressure loss coefficients, their spanwise total pressure distributions exhibit a similar picture as found by Berg (1973). Figures 11a, b, and c present the total pressure contour plots at stations 3, 4, and 5. The contour plot of the total pressure distribution downstream of the first rotor, at station 3, is shown in Figure 11a. Three distinct flow regions are visible in this figure. At the hub and tip, relatively thin low total pressure regions indicate the presence of wall boundary layer with low total pressure fluid. Close to the hub, a slightly lower total pressure region is visible, which is caused by the combined effect of secondary flow and mixing. In the center, another region of slightly lower total pressure indicates the presence of relatively thick wakes. As stated previously, pneumatic (five-hole) probes were used for this investigation. These probes inherently have low frequency response, however, the flow within the axial gaps is highly unsteady. To capture the flow details, high frequency response probes such as hot wire probes are required. A more conclusive picture of the total pressure distribution is given by Figure 11b. In addition to the thin, low energetic boundary layer zones at the hub and tip, Figure 11b reveals a relatively thick wake region immediately downstream of the stator blade trailing edge. Outside the wake region, the flow exhibits an insignificant total pressure variation which indicates that secondary flow vortices do not predominate the flow field leading to substantial total pressure losses. Downstream of the second rotor at station

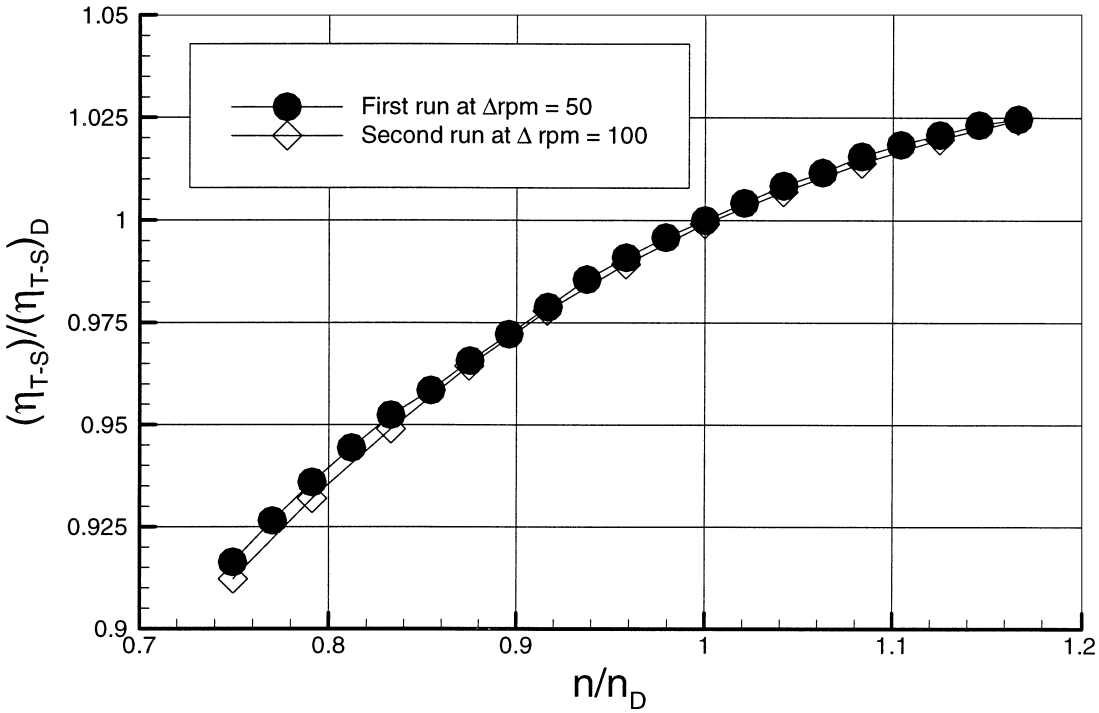

FIGURE 12
Normalized efficiency as a function of normalized frequency.

5, the total pressure contour, Figure 11c, is almost identical with the one downstream of the first rotor discussed previously.

Efficiency Measurements, Results

The total to static efficiency was obtained using the net turbine power measured by the torque meter and taking into account the bearing and windage losses. To show the performance behavior of the turbine engine, normalized efficiency diagrams are generated with respect to the design point condition. Keeping the engine pressure ratio and the turbine inlet temperature constant, the engine rotational speed was varied from 75% to 116% of the design operating speed. To insure the test repeatability, two final efficiency tests were run. Figure 12 represents the normalized efficiency as a function of normalized engine rotational speed. As this figure reveals, a pronounced efficiency drop is observed for off-design operating points. A deviation from the design rotational speed by −10% results in an efficiency decrease of more than 3%. However, increasing the rotational speed by 10% causes the efficiency to increase by slightly more than 1%. The variation of the efficiency over the speed range is mainly due to the change in the absolute exit flow angle, which determines the exit losses. The efficiency results presented above show how important the design point efficiency prediction is.

CONCLUSION

A three-stage turbine research facility, established very recently at the Texas A&M University, Turbomachinery Performance and Flow research Laboratory (*TPFL*) was introduced and described. This article exhibits the first part of a series of papers that deal with turbine performance and flow research issues. It presents the results of the experiments performed on a three-stage HP-turbine with 3-D blades. As the first test case, shrouded three-dimensional stator and rotor blade rows were used for flow and efficiency measurements. The results of the interstage traversing taken downstream of the first rotor, second stator, and second rotor row were presented. The normalized stator and rotor total pressure loss coefficient indicates a reduced effect of secondary flow losses in the hub and tip region. Performance and efficiency measurements were carried out within a rotational speed range of 75% to 116% design rotational speed. A pronounced efficiency drop is observed for off-design operating points. A deviation from the design rotational speed, by −10%, resulted in an efficiency decrease of more than 3%. However, increasing the rotational speed by 10% caused the efficiency to increase by slightly more than 1%.

NOMENCLATURE

Bh	blade height (mm)
D	diameter (mm)
$\dot{m}$	dot mass flow (kg/s)
M	Mach number (−)
n	rotational speed (rpm)
p	static pressure (kpa)
P	total pressure (kpa)
α	absolute flow angle (°)

β relative flow angle (°)
ζ total pressure loss coefficient
ζ_0 design point total pressure loss coefficient

REFERENCES

Arndt, N. 1993. Blade row interaction in a multistage low pressure turbine. *ASME Journal of Turbomachinery* 115:137–146.

Berg, H. 1973. *Untersuchungen über den Einfluß der Leistungszahl auf Verlusten in Axialturbinen*. Dissertation, Facultät Maschinenbau, Technische Hochschule Darmstadt, D17.

Chakka, P., and Schobeiri, M. T. 1999. Modeling of unsteady boundary layer transition on a curved plate under periodic unsteady flow condition: Aerodynamic and heat transfer investigations. *ASME Transactions, Journal of Turbo Machinery* 121: 88–97.

Day, C. R. B., Oldfield, M. L. G., and Lock , G. D. 1999. The influence of film cooling on the efficiency of an annular nozzle guide vane cascade. *ASME Transactions, Journal of Turbomachinery* 121:145–151.

Dzung, L. S. 1971. Konsistente mittewerte in der theorie der turbomaschinen für kompressible medien. *BBC-Mitteilung* 58:485–492.

Emunds, R., Jennions, I. K., Bohn, D., and Gier, J. 1999. The computation of adjacent blade-row effects in a 1.5-stage axial flow turbine. *ASME Transactions, Journal of Turbo Machinery* 121:1–10.

Halstead, D. E., Wissler, D. C., Okiishi, T. H. et al. 1995. Boundary layer development in axial compressors and turbines. *ASME-papers: 95-GT-461-463, Part 1, 2, 3, and 4*.

Hodson, H. P., Hustman, I., and Steele. 1993. An investigation of boundary layer development in a multistage LP turbine. *ASME Paper No. 93-GT-310*.

Schobeiri, M. T., John, J., and Pappu, K. 1994. Development of two-dimensional wakes within curved channels, theoretical framework and experimental investigation. *ASME Transactions, Journal of Turbomachinery* 118:506–518.

Schobeiri, M. T., Pappu, K., and John, J. 1995a. Theoretical and experimental study of development of two-dimensional steady and unsteady wakes within curved channels. *ASME Transactions, Journal of Fluid Engineering* 117:593–598.

Schobeiri, M. T., Read, K., and Lewalle, J. 1995b. Effect of unsteady wake passing frequency on boundary layer transition, experimental investigation and wavelet analysis. *ASME 95-GT-437*, presented at the International Gas Turbine and Aero-Engine Congress and Exposition, Houston, Texas, June 5–8, 1995.

Schobeiri, M. T., Chakka, P., and Pappu, K. 1998. Unsteady wake effects on boundary layer transition and heat transfer characteristics of a turbine blade. *ASME paper: 98 GT-291*, presented at the IGTI Gas Turbine and Aeroengine Congress & Exhibition, Stockholm, June 2–5, 1998.

Schütz, J. 1971. *Beitrag zur Berechnung der Strömung in Stufen axialer thermischer Turbomaschinen*. Dissertation, Facultät Maschinenbau, Technische Hochschule Darmstadt, D17.

Traupel, W. 1977. *Thermische Turbomaschinen*. Berlin, Heidelberg, New York: Auflage, Springer Verlag.

Wright, L., and Schobeiri, M. T. 1999. The effect of periodic unsteady flow on boundary layer and heat transfer on a curved surface. *ASME Transactions, Journal of Heat Transfer* 120:22–33.